

RSC Advances



This is an *Accepted Manuscript*, which has been through the Royal Society of Chemistry peer review process and has been accepted for publication.

Accepted Manuscripts are published online shortly after acceptance, before technical editing, formatting and proof reading. Using this free service, authors can make their results available to the community, in citable form, before we publish the edited article. This *Accepted Manuscript* will be replaced by the edited, formatted and paginated article as soon as this is available.

You can find more information about *Accepted Manuscripts* in the [Information for Authors](#).

Please note that technical editing may introduce minor changes to the text and/or graphics, which may alter content. The journal's standard [Terms & Conditions](#) and the [Ethical guidelines](#) still apply. In no event shall the Royal Society of Chemistry be held responsible for any errors or omissions in this *Accepted Manuscript* or any consequences arising from the use of any information it contains.

Enhanced dielectric properties and energy storage density in poly(vinylidene fluoride-co-hexafluoropropylene) by relaxor ferroelectric ceramic

Hang Luo, Chao Chen, Kechao Zhou*, Xuefan Zhou, Zhong Wu, and Dou Zhang*

State Key Laboratory of Powder Metallurgy, Central South University, Changsha, Hunan 410083, China

*E-mail: dzhang@csu.edu.cn (D. Zhang);

*E-mail: zhoukechao@csu.edu.cn (C. Zhou)

KEYWORDS: dielectric properties, energy storage, composites, surface-functionalized, relaxor ferroelectric ceramic

Abstract

In this work, relaxor ferroelectric ceramic $0.67\text{Pb}(\text{Mg}_{1/3}\text{Nb}_{2/3})\text{O}_3-0.33\text{PbTiO}_3$ (PMN–PT) was synthesized by molten–salt growth method, which have lower remnant polarization and slimmer hysteresis loops than traditional ferroelectric ceramics. The PMN–PT particles maintained homogeneous dispersion in the composite and adhered tightly with poly(vinylidene fluoride-co-hexafluoropropylene) (P(VDF-HFP)) matrix due to the modification of dopamine. The composites had a maximum dielectric constant of 65.1 and a low dielectric loss of less than 0.037 at 1 kHz. Due to the low remnant polarization of the relaxor ferroelectric ceramic of PMN–PT, the energy density of the composites was significantly increased. The discharged energy density of the sample with 50 vol% PMN–PT was 4 times of P(VDF-HFP) at 80 kV/mm. It was demonstrated that the dopamine functioned PMN–PT/P(VDF-HFP) composite was a potential dielectric materials in the future application of energy storage.

Introduction

Dielectric materials with high discharged energy density have attracted scientific and commercial interest due to the prospect of application on electronic devices such as radar, lasers, defibrillators, rail guns, and pace makers.¹⁻⁵ However, the technologies in current states suffer from low energy density, which make them bulky and costly. One of the desirable strategy to increase the energy density of these materials is to apply 0–3 type inorganic/polymer composites (zero-dimensional fillers in a three-dimensionally connected polymer matrix), because they hold high dielectric strength and excellent processability of the polymer, which overcome the limitations associated with the conventional inorganic ceramic and organic dielectric materials.⁶⁻¹³ In general, the discharged energy density (J) of dielectric materials is related to the equation as:

$$J = \int_{D_r}^{D_{\max}} E dD \quad (1)$$

where D_{\max} and D_r are the maximum electric displacement and remnant electric displacement of the materials, respectively, E is the applied electric field. Electric displacement (D) is defined as:

$$D = \varepsilon_0 \varepsilon_r E \quad (2)$$

where ε_0 and ε_r are dielectric constant of vacuum and the relative dielectric constant of the dielectric materials, respectively. It can be seen that the J can be increased by simultaneously increasing dielectric constant and breakdown strength.¹⁴¹⁵ Thus, finding a material with high dielectric constant and dielectric strength without a large increase in dielectric loss is the key factor to promote the development of

dielectric materials on the application of energy storage.¹⁶

Generally, ferroelectric ceramics, such as $\text{Pb}(\text{Zr}, \text{Ti})\text{O}_3$ (PZT), BaTiO_3 , etc., have often been chosen as the fillers in polymer composites due to their high dielectric constants.¹⁷⁻¹⁹ While the ferroelectric ceramics always suffer from fat hysteresis loops with high coercive electric field and high remanent polarization, which would decrease the discharged energy density and energy efficiency.²⁰⁻²² In contrast, relaxor ferroelectric ceramics, such as $(\text{Ba}, \text{Sr})\text{TiO}_3$, La-doped PZT, and $\text{Pb}(\text{Mg}_{1/3}\text{Nb}_{2/3})\text{O}_3$ - PbTiO_3 (PMN-PT) exhibit higher dielectric constant, relatively low remnant polarization and slim hysteresis loops in comparison to traditional ferroelectric ceramics.^{22, 23} Nowadays, a lot of attentions have been paid on relaxor ferroelectric ceramics for energy storage application. Brown et. al., reported a kind of relaxor ferroelectric ceramic of La-doped PZT for energy storage applications. Due to the relatively low remanent polarization and coercive electric field, a maximum energy density of 13.3 J/cm^3 with an energy efficiency of 77% was obtained.²⁴ Similarly, Hao et al., achieved a maximum energy density of 28.7 J/cm^3 in La-doped PZT films with the thickness of $1 \mu\text{m}$ on platinum-buffered silicon substrates.²⁵ Wu et. al., reported a novel relaxor ferroelectric capacitor of $\text{BaTiO}_3@ \text{SrTiO}_3$ ceramic with core-satellite structure, which largely enhanced energy storage density and improved energy efficiency compared with the ferroelectric BaTiO_3 .²⁶ Much attention were paid to the relaxor ferroelectric ceramics for energy storage, however, flexible relaxor ferroelectric ceramic/polymer composites with high dielectric constant of the relaxor ceramics and high dielectric strength of the polymer matrix are overlooked. Therefore,

introducing relaxor ferroelectric ceramics to polymer matrix would be meaningful to prepare flexible dielectric materials with improved discharged energy density and energy efficiency.

In this paper, relaxor ferroelectric PMN–PT ceramic particles were synthesized by molten-salt growth method. The synthesized PMN–PT ceramic particles were modified by dopamine before being introduced to the poly(vinylidene fluoride-co-hexafluoropropylene) (P(VDF-HFP)) matrix. Compared with the pristine PMN–PT, the modified PMN–PT particles dispersed homogeneously in the composites, strong interfacial adhesion with the polymer matrix and the composite showed improved dielectric properties with modified PMN–PT particles. The energy density storage of the composites was as high as 1.02 J/cm^3 , which is more than four times over the pure P(VDF-HFP) matrix. The findings of this research could provide an effective approach to build high energy density storage capacitors.

Experimental section

Materials

The chemicals were obtained from the following sources and used without further purification: PbO (kermel, China, 99%), Nb₂O₅ (Sinopharm, China, 99%), [(MgCO₃)₄Mg(OH)₂]5H₂O (Sinopharm, China, 99%), TiO₂(Anatase, Aladdin, 99.8%), KCl(Sinopharm, China, 99.5%). Dopamine hydrochloride (Alfa, 99%), P(VDF-HFP) (Aldrich, pellets with less than 15% of HFP), and other reagents are all analytically pure.

Synthesis of PMN–PT powders by molten-salt growth method

11.5 g of PbO (51.5 mmol, excess 3%), 1.07 g of $[(\text{MgCO}_3)_4\text{Mg}(\text{OH})_2]5\text{H}_2\text{O}$ (2.2 mmol), 2.95 g of Nb_2O_5 (11.1 mmol), 1.33 g of TiO_2 (16.7 mmol) and 17 g of KCl (228.2 mmol) were mixed in the media of ethyl alcohol by ball-milling with the speed of 150 r/min for 12 h. The mass ratio of the raw material, media and ball was 1:1:1.5. The sintering process was done under 850 °C for 1 h, afterwards, the production was soaked in the water under 80 °C for 24 h. The soaked content was undergone heat treatment under 650 °C for 1 h after suction filtration. The PMN-PT powder with compositions of $0.67\text{Pb}(\text{Mg}_{1/3}\text{Nb}_{2/3})\text{O}_3-0.33\text{PbTiO}_3$ was finally obtained by planetary ball-milling for 4 days.

Functionalization of the PMN-PT particles

Dopamine modified PMN-PT was prepared using a method reported previously.²⁷ In a typical reaction, 10 g of PMN-PT particles was dispersed in 100 mL mixture of 95:5 (v/v) ethanol/ H_2O by an ultrasonic processor to increase the hydroxyl on the surfaces of PMN-PT. The PMN-PT particles were recovered by centrifugation and dried under vacuum at 60 °C for 12 h. The hydroxylated PMN-PT particles were dispersed in 0.01 M of dopamine hydrochloride aqueous solution and stirred for 10 h at 60 °C. The particles were separated by centrifugation and rinsed repeatedly with excess deionized water. Afterwards, the functionalized PMN-PT particles were dried overnight under vacuum at 60 °C.

Fabrication of the PMN-PT/P(VDF-HFP) composites

Functionalized PMN-PT particles were ball-milled in *N,N*-dimethylformamide (DMF) for 2 days, and mixed with P(VDF-HFP) for another 5 days by ball-milling.

The resultant suspension was then casted onto a clean glass, and dried at 80 °C for 12 h under vacuum. The dried composites sheets were compressed into films at 200 °C under a pressure of about 15 MPa. Gold electrodes were sputtered on both sides of the film using a mask with 2 mm diameter eyelets.

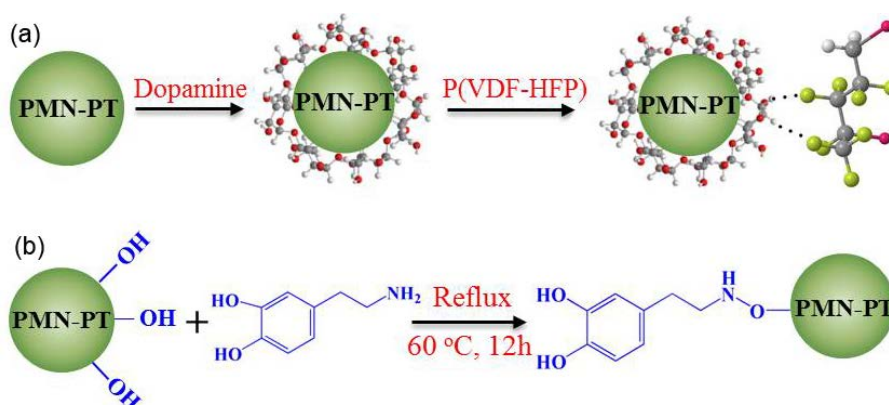


Fig. 1 Schematic diagrams of (a) modified PMN–PT particles by dopamine in P(VDF-HFP) composite and (b) the reaction between the PMN–PT particles and dopamine.

The fabrication process of PMN–PT/P(VDF-HFP) composites is shown in Fig. 1. As the image showed, the PMN-PT particles were firstly modified by dopamine. The chemical structure of dopamine contains OH groups and NH₂, which could interact strongly with a variety of inorganic particles by hydrogen bonding.²⁸ In addition, Dopamine could forms strong covalent and noncovalent interactions with substrates.²⁹ As shown, the polymerization reaction of dopamine took place on the particle surfaces.³⁰⁻³² The functional PMN–PT particles were then dispersed in the P(VDF-HFP) solution by ball-milling. The modifier adhered tightly on the surfaces of the PMN–PT, meanwhile, the organics layer bonded tightly with the polymer matrix due to the presence of strong electron-withdrawing functional group (–C–F) of

P(VDF-HFP). Afterwards, the composite films were prepared as reported previously.⁷

Characterization

The crystal structure of the ceramic and composites was examined in θ - 2θ mode by X-ray diffraction (XRD, Rigaku D-Max/2550VB⁺) utilizing Cu K_{α} radiation ($\lambda=1.5418 \text{ \AA}$). Fourier-transform infrared (FT-IR) spectroscopy was performed with a Nicolet 6700 instrument over the range of $4000\text{--}450 \text{ cm}^{-1}$ to determine the functionalization of the samples. Transmission electron microscopy (TEM) images were obtained from a Titan G2 60–300 instrument operated at an accelerating voltage at 300 kV. Thermogravimetric analysis (TGA, NETZSCH STA 449) was conducted at a heating rate of $10 \text{ }^{\circ}\text{C}/\text{min}$ in a nitrogen flow ($20 \text{ ml}/\text{min}$). The morphology of the composites was performed by scanning electron microscopy (SEM, JSM–6390). Frequency–dependent dielectric constant and dielectric loss were measured using an Agilent 4294A LCR meter with a frequency range from 100 Hz to 10 MHz. Electric displacement–electric field loops and leakage current were measured by a Precision Premier II ferroelectric polarization tester (Radiant, Inc.) at room temperature and 100 Hz.

Results and Discussion

Characterization of pristine PMN-PT and dopamine modified PMN-PT particles

Fig. 2 exhibits the X-ray diffraction pattern of the PMN–PT particles. It was shown that the strong peaks at 2θ of 22, 31, 39, 45, 51, and 56 can be corresponded to (100), (110), (111), (200), (210) and (211) characteristic peaks of PMN–PT with cubic crystalline. All of the peaks were matched well with perovskite peaks based on the

powder diffraction file database (#80–1351). These peaks indicated that a pure perovskite phase is obtained in the PMN–PT particles by molten-salt growth method. The morphologies of the PMN–PT particles were revealed by SEM image, which was inserted in Fig. 2. As can be seen, the particles showed irregular shapes and wide distribution of the size. The average diameter was about 320 nm, which was measured by laser particle size analyzer. The results were attributed to the limit of the mechanical ball-milling.

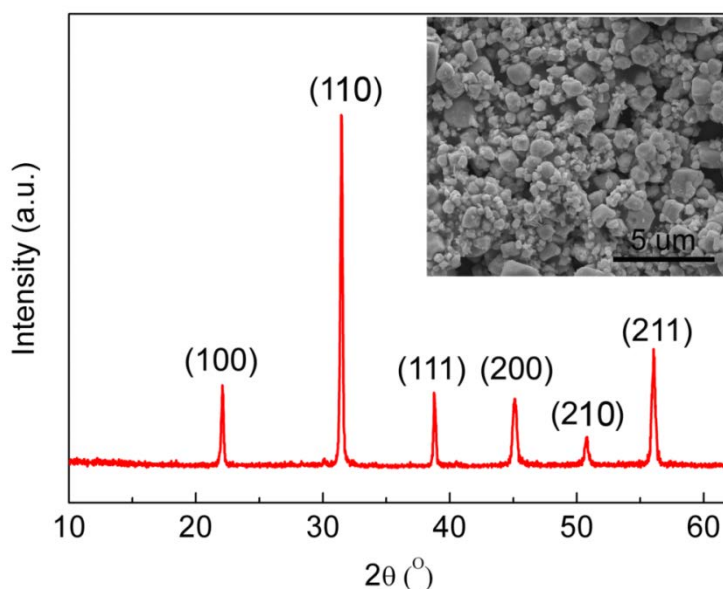


Fig. 2 X-ray diffraction pattern of the PMN–PT ceramic particles. The inset is SEM image of the PMN–PT particles.

The FT-IR absorbance spectra of pristine PMN–PT particles, dopamine modified PMN–PT particles, and pure dopamine is shown in Fig. 3. The absorption intensity in the range of $3800\text{--}800\text{ cm}^{-1}$ wavenumbers increased after the PMN–PT particles are modified by dopamine. A broad absorbance band between $3500\text{ and }3000\text{ cm}^{-1}$ appears after the surface modification, which corresponds to O–H and/or N–H

stretching vibrations derived from dopamine.³³ The absorption peaks located at 1616 and 1286 cm^{-1} wavenumbers came from the N–H bending vibrations and aromatic amine C–N stretching vibrations, respectively, which were generated from aromatic and amino groups. While the absorption peaks were not appeared in the sample of pristine PMN–PT particles. In addition, the absorption peaks located at 1680 cm^{-1} in was only appeared in the sample of dopamine modified PMN–PT, which indicated that a new covalent bond of N–O was formed. The results implied that dopamine was exited in the surfaces of the functionalized PMN–PT particles.

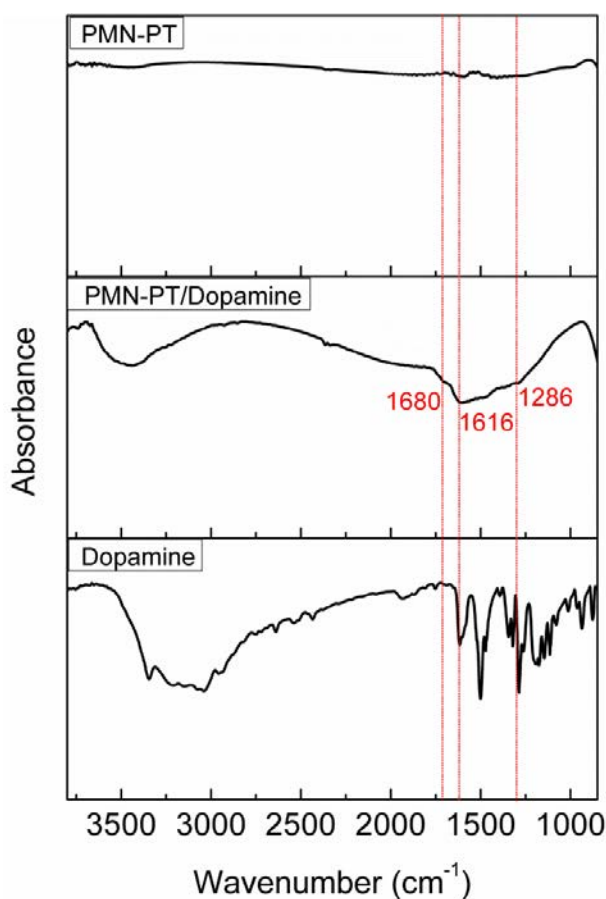


Fig. 3 The FT-IR spectra of PMN–PT, modified PMN–PT by dopamine and pure dopamine.

Fig. 4a displays the TEM image of the functionalized PMN–PT particle with

dopamine. A polymer layer with the thickness of ~ 7 nm can be clearly observed on the surface of the PMN–PT particle. The corresponding high-resolution image of the functionalized PMN–PT particle is exhibited in Fig. 4b. An obvious interface with discrepant high resolution stripe can be seen in the two sides of the interface, which was agreed with the result in Fig. 4a. Fig. 4c shows the TGA curves of pristine PMN–PT, functionalized PMN–PT particle, and the pure dopamine. The amount of the dopamine coated on the surfaces of the PMN–PT particle is characterized by TGA. The net weight loss of functionalized PMN–PT is found to be 3.2%, which was attributed to the coated dopamine because the weight loss of pure dopamine was about 75 %, while the pristine PMN–PT almost had no weight loss.

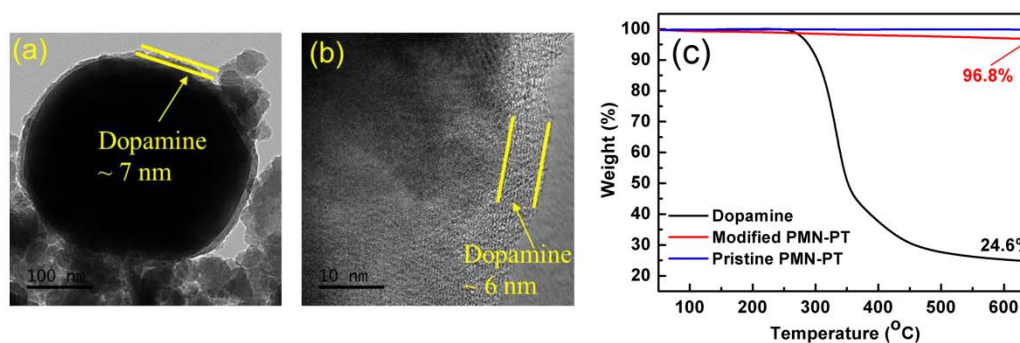


Fig. 4 (a) Bright-field image, and (b) HR-TEM image of a PMN–PT particle after surface modification by dopamine. (c) TGA curves for the pristine PMN–PT, modified PMN–PT by dopamine, and pure dopamine.

Characterization of the PMN–PT/P(VDF-HFP) composites

The microscopic homogeneity of the PMN–PT/P(VDF-HFP) composite films is investigated by imaging the cross sections, which are shown in Fig. 5. Among the

SEM images, the content of the PMN–PT particles in samples (a), (b) and (c) were 10 vol%, 30 vol% and 50 vol%. Samples (d), (e) and (f) separately had the same content of the PMN–PT with samples (a), (b) and (c). While the difference was the PMN–PT particles in samples (d), (e) and (f) were modified by dopamine before being introduced to the polymer matrix. A small amount of particles were observed in the composites when the content of PMN–PT was 10 vol%, which were shown in Fig. 5a and 5d. The visible particles in the composites were more and more intensive with the increase of the loadings of PMN–PT. It can be clearly seen that the PMN–PT without modification exhibited poor compatibility with P(VDF-HFP) matrix, the particles were scattered in the matrix without bonding force, and more and more defects were found in the composites with the increase of the loadings of PMN–PT. Satisfyingly, the problems were distinctly improved after the PMN–PT particles being modified by dopamine. As can be seen in Fig. 5d–5f, the particles were uniformly embedded in the polymer matrix with strong bonding force and neglected evidence of defects were observed even when the loading of PMN–PT reached 50 vol%. Due to larger interfacial areas between the polymer matrix and the particles in the composites than the unmodified particles was obtained, which would promote the coupling effect through a dipolar interface layer and result in higher polarization and dielectric response.^{33, 34} Thus, PMN–PT modified by dopamine is benefit to enhance the dielectric properties and energy storage capacity of the composite.

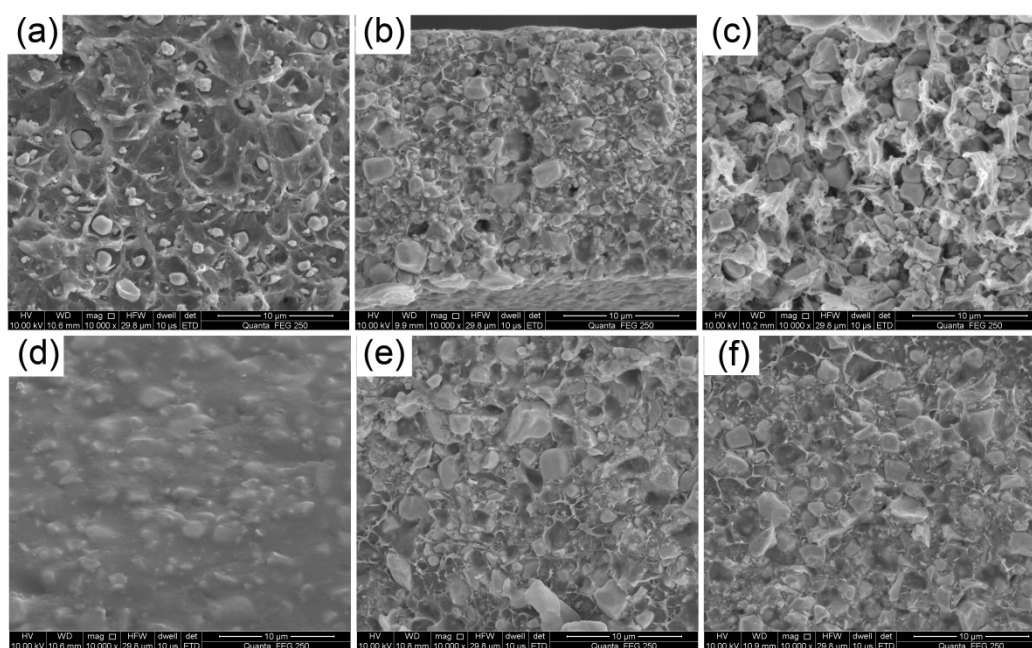


Fig. 5 SEM images of the cross sections of the composites with (a) 10 vol%, (b) 30 vol%, (c) 50 vol% PMN–PT particles, and (d) 10 vol%, (e) 30 vol%, (f) 50 vol% dopamine modified PMN–PT particles.

Fig. 6a shows the XRD patterns of pure P(VDF-HFP) and PMN–PT/P(VDF-HFP) composites with different amount of PMN–PT. It can be seen that the XRD pattern of the pure P(VDF-HFP) exhibited an intense scattering background and a wide hump at about 20° , which was a typical feature of amorphous structure. Both diffraction peaks from perovskite structure of PMN–PT ceramics and scattering hump from P(VDF-HFP) matrix can be observed in the composite films. XRD pattern of the composites showed the diffraction peaks located at 22° , 31° , and 39° , which can be attributed to the (100), (110), and (111) reflections of PMN–PT (no. #80–1351). However, as shown in the dotted box that the diffraction peaks of P(VDF-HFP) became more and more negligible in the composites with the increase of the loadings of PMN–PT. This result indicated that the introduction of PMN–PT particles destroy

the crystallization of the P(VDF-HFP) matrix, and the amorphous degree is higher and higher with the increase of the loadings of PMN–PT particles.³⁵ The DSC curves of the samples obtained during the heating scan process are presented in Fig. 6b. As can be seen that the crystallization temperature increased by 4.5 °C with the introduction of PMN–PT particles, which was 155.9 °C for the P(VDF-HFP) to 160.4 °C for the composite with 10 vol% PMN–PT particles. However, the crystallization temperature decreased with the increase of the PMN–PT loadings. The PMN–PT fillers effect the crystallization temperature of P(VDF-HFP) composites mainly due to two reasons. One reason is that the PMN–PT fillers in the composite acted as the new nucleation center, which can decrease the nucleation energy and increase the degree of crystallization of the P(VDF-HFP) matrix for the crystallization of P(VDF-HFP) on the surfaces of PMN–PT. Another reason is that the introduction of PMN–PT fillers decreased the degree of the order of P(VDF-HFP) matrix, which means that the degree of crystallization of the P(VDF-HFP) matrix was decreased. Thus, the crystallization temperature of P(VDF-HFP) increased with the small amount of PMN–PT particles, while it decreased with increasing the particle loadings.

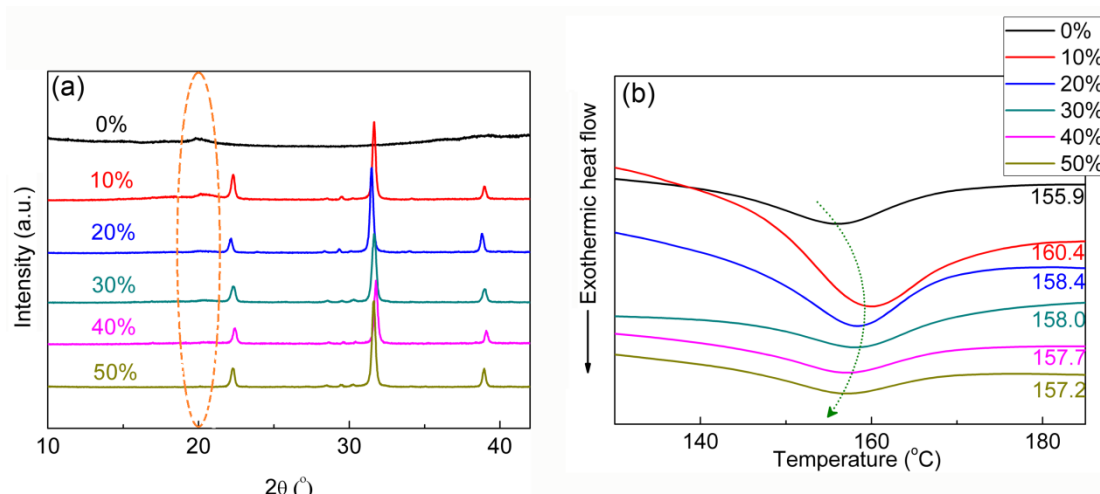


Fig. 6 (a) XRD patterns of PMN–PT particles, pure P(VDF–HFP), and PMN–PT/P(VDF–HFP) composites with different volume fractions of BT. (b) DSC curves of the samples during the heating cycle at a rate of 10 $^\circ\text{C}/\text{min}$ under N_2 atmosphere.

Dielectric properties and Energy Storage Performance of the PMN–PT/P(VDF–HFP) Composites

To further discuss the effect produced by dopamine on the dielectric properties, frequency dependence of dielectric properties of the compared composites with unmodified PMN–PT and modified PMN–PT respectively are shown over the range of 100 Hz to 100 MHz, which is exhibited in Fig. 7. As can be seen, the composites with modified PMN–PT fillers had improved dielectric properties than the composites with unmodified PMN–PT fillers. The maximum dielectric constant of the composite with modified PMN–PT was increased from 8.3 to 65.1, while the composite with unmodified fillers was 53.5. High dielectric constant of composites mainly arised from the MWS interfacial effect,³⁶ PMN–PT fillers modified by dopamine exhibited uniform dispersion in the composite, which resulted in larger interfacial areas between

PMN–PT particles and P(VDF-HFP) matrix than the composite with unmodified fillers. It is noted that the composites with modified PMN–PT held extremely low dielectric loss, which was less than 0.037 at 1 kHz at room temperature. The changing trend of the dielectric loss in the high frequency range was the same with the degree of crystalline of the polymer matrix, which was increased in the first and then decreased, as shown in Fig. 6b and Fig. 7d. The dielectric loss of the composites with unmodified PMN–PT obviously increased, which even increased to 0.103 when the composite with 50 vol% unmodified PMN–PT. This result can be understood from the results of the comparison in Fig. 5, which showed much voids and defects in the composite with unmodified PMN–PT.

The effective dielectric constant (at 1 kHz) of the composites as a function of PMN–PT particles volume fraction compared with the predicted values from different theoretical models is shown in Fig. 7e. The experimental dielectric constant gradually increased with the increase of the filler volume fraction. A large discrepancy between experimental value and calculated value from Maxwell-Garnett model was observed when the particles content is more than 20 vol%. This is due to the interaction among the particles become more and more serious with the increase of the PMN–PT particles content. However, the experiment results agree well with the value from Jayasundere–Smith model.

Fig. 7f shows the frequency dependence of the electric conductivity for the composites with modified PMN–PT fillers. The samples showed relative low electric conductivity, especially when the loading of the PMN–PT fillers was 10 vol% and 20

vol%, which was even lower than the pure P(VDF-HFP). The reason was attributed to the dopamine insulating shell on the surfaces of PMN-PT particles, which restricted the migration and accumulation of the space charge within the composite. However, the electric conductivity of the composite increased obviously when the loading of PMN-PT was larger than 20 vol%. For example, the electric conductivity of the sample with 10 vol% PMN-PT was 1.8×10^{-6} S/m, and the sample with 50 vol% PMN-PT was 9.3×10^{-6} S/m at 1 kHz. Unavoidable defects such as the agglomerations, voids and cracks would be produced in the composites when the loading of PMN-PT was high, which lead to the increase of the electric conductivity.

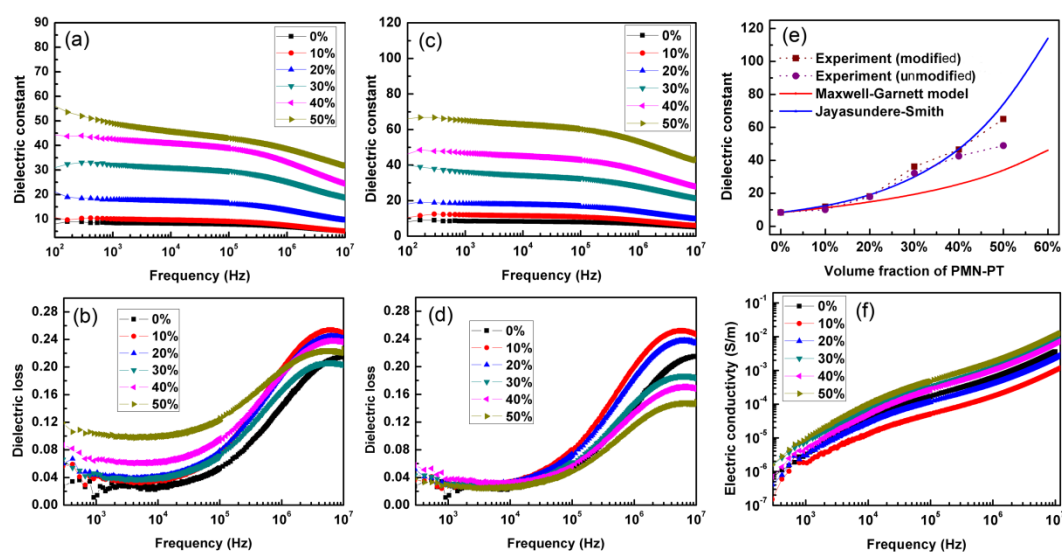


Fig. 7 Frequency dependence of (a) dielectric constant, (b) dielectric loss of the P(VDF-HFP) composites with unmodified PMN-PT, (c) dielectric constant, (d) dielectric loss, and (f) electric conductivity of the P(VDF-HFP) composites with modified PMN-PT at room temperature. (e) Comparison of measured effective relative dielectric constant (at 1 kHz) of the composites as a function of PMN-PT particles volume fraction with predicted values from different theoretical models.

The frequency dependence of imaginary electric modulus (M'') of the composites

$$M'' = \varepsilon'' / (\varepsilon'^2 + \varepsilon''^2) \quad (3)$$

and the pure P(VDF-HFP) at room temperature is shown in Fig. 8, where ε' and ε'' are correspond to the real and imaginary parts of the complex dielectric constant of the samples, respectively. The relaxation intensity of the samples was decreased and become broader with the introduction of PMN-PT compared to the P(VDF-HFP), which was especially obvious when the content of the PMN-PT reached to 30 vol%. The result was due to the PMN-PT fillers restrained the space charge aggregation in the composites,³⁷ and is consistent with the low conductivity of the composites showed in Fig. 7c. The relaxation peaks were appeared at high frequency range ($\sim 10^7$ Hz), which would be attributed to the movement and accumulation of free charges result from dipole relaxation of the P(VDF-HFP) matrix at high frequency range,^{7, 38} and was agreed with the trend of the dielectric loss. While the peaks shift to direct of the lower frequency with the increase of the PMN-PT content. For example, the relaxation peaks of the sample with 10% PMN-PT content is at about 2×10^7 Hz, which was moved to about 9×10^6 Hz when the PMN-PT content was increased to 50 vol%.

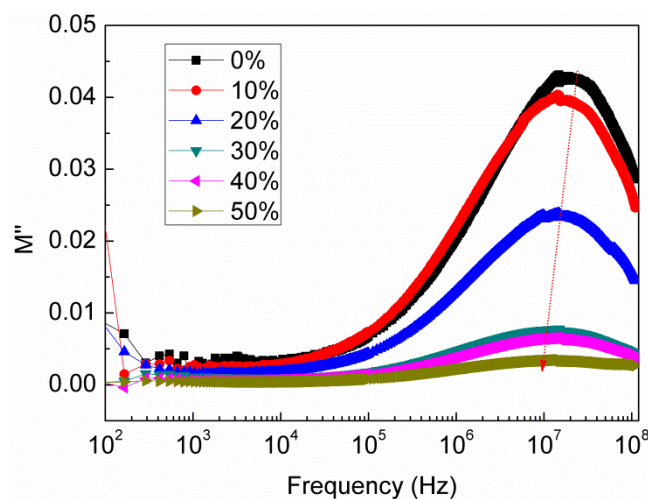


Fig. 8 Frequency dependence of the imaginary electric modulus of the samples with varied content of PMN–PT particles at room temperature.

Discharged energy density is related to not only dielectric constant but also breakdown strength of the composite. The results in Fig. 9 show the comparison of breakdown strength between the composites with modified PMN–PT by dopamine and unmodified PMN–PT as a function of the loadings of PMN–PT. The composites with modified PMN–PT particles have higher breakdown strength than the composites with unmodified PMN–PT. The breakdown strength of the composites with modified PMN–PT orderly were 200, 167, 152, 129, and 83 kV/mm. For comparison, of which with unmodified PMN–PT were 188, 150, 148, 74, and 67 kV/mm. These can be attributed to better quality of the composite films after the modification by dopamine. As Fig. 5 clearly showed that the modified composite films had no obvious aggregation and ignorable defects. In addition, the breakdown strength decreased with the increase of PMN–PT loadings, which showed 325 kV/mm for the pure P(VDF-HFP), decreased to 152 kV/mm for the composite with 30 vol% PMN–PT particles, and decreased to 83 kV/mm when the loading of PMN–PT

increased to 50 vol%. Similar phenomenon was also shown in the composites with unmodified PMN–PT. The agglomerations and voids in the composites were more and more with the increase of PMN–PT, which resulted in inhomogeneous electric field breakdown strength in the polymer matrix and lead to the decrease of the effective breakdown strength of the composites.^{39, 40}

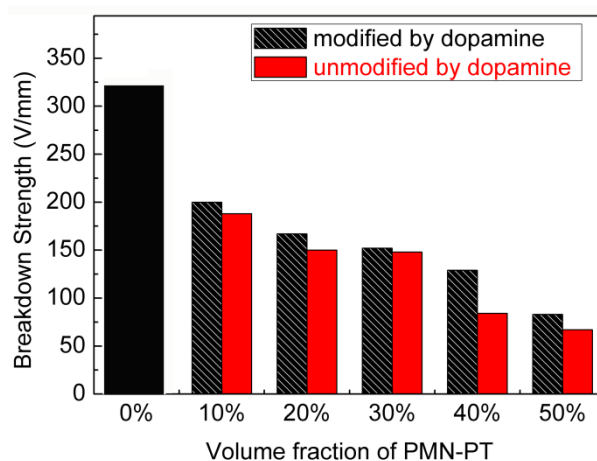


Fig. 9 The comparison of breakdown strength between the composites with modified PMN–PT by dopamine and unmodified PMN–PT as a function of the loadings of PMN–PT.

According to the equation (1), J can be derived from the electric displacement–electric field (D – E) loops.^{41, 42} Typical D – E loops of the composites with various volume fractions of modified PMN–PT particles were measured at the electric field of 80 kV/mm, which were shown in Fig. 10a. It is shown that the electric displacement increased notably with the increase of the loadings of PMN–PT fillers. The detail performances of the composites originated from the D – E loops were shown in Table 1. As can be seen that the electric displacement of the samples were 0.64, 1.94, 2.25, 3.26, 3.86, and 6.61 $\mu\text{C}/\text{cm}^2$. According to equation (2), the increased electric

displacement was due to the increase of dielectric constant of the samples, which was consistent with the results in Fig. 7c.

The energy density of the samples as a function of the loadings of PMN-PT fillers is shown in Fig. 10b. As can be seen, the energy density increased with the increase of the content of the PMN-PT fillers. The energy density of the pure P(VDF-HFP) was 0.25 J/cm^3 at 80 kV/mm , and increased to 1.02 J/cm^3 when the PMN-PT loading increased to 50 vol% at the same electric field, which was increased by about 3 times. Due to the improved dielectric properties of the composites with modified PMN-PT fillers, which led to higher energy density than the composites with unmodified PMN-PT. Additionally, the PMN-PT/P(VDF-HFP) composite films exhibited excellent flexibility, which can be demonstrated by the digital photo inserted in Fig. 10b. Although the relaxor ferroelectric properties was not exhibited by the samples, the relaxor ferroelectric ceramics (PMN-PT, BST, etc.) composite with polymer for energy storage application is still deserve further study.

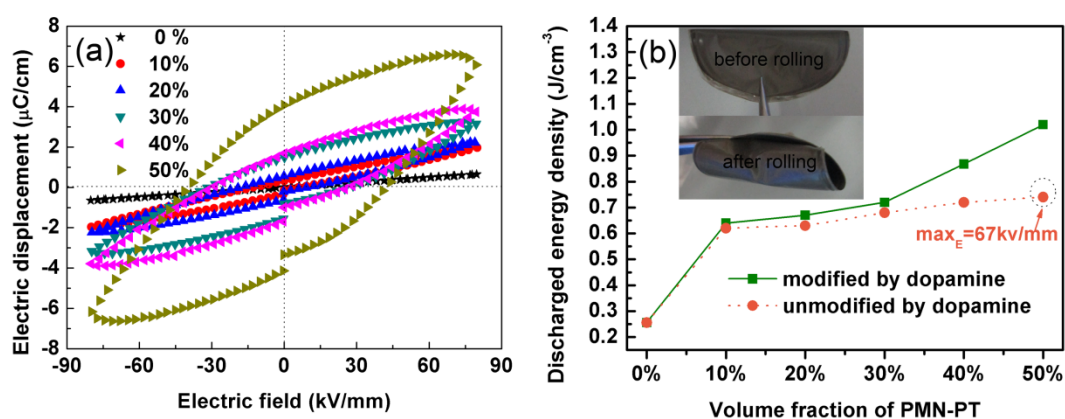


Fig. 10 (a) D - E loops and (b) discharged energy densities of the samples at the electric field of 80 kV/mm . The difference is the electric field of the composite with 50 vol% unmodified PMN-PT is 67 kV/mm . The inset in (b) is the digital photos of

flexible composite before rolling, and after rolling.

Table 1. The performances of the composites with the modified PMN–PT particles by dopamine at the electric field of 80 kV/mm.

No.	D_{\max} ($\mu\text{C}/\text{cm}^2$)	D_r ($\mu\text{C}/\text{cm}^2$)	U_{\max} (J/cm^3)
0%	0.64	0.01	0.25
10%	1.94	0.32	0.64
20%	2.25	0.57	0.67
30%	3.26	1.47	0.72
40%	3.86	1.69	0.86
50%	6.61	4.06	1.02

Conclusions

Relaxor ferroelectric ceramic PMN–PT ceramics were synthesized, and introduced to ferroelectric polymer P(VDF-HFP). The modified PMN–PT particles maintained homogeneous dispersion in the composite and adhered tightly with P(VDF-HFP) matrix. Due to the high-quality composite films, the composites with modified PMN–PT exhibited significantly superiority on enhancing the dielectric properties and energy storage density compared with the pure P(VDF-HFP) and the composites with unmodified PMN–PT. The maximum dielectric constant of the composites was up to 65.1, compared to 8.3 of the P(VDF-HFP) at 1 kHz. Meanwhile, the increased dielectric constant was not at the expense of increase of the dielectric loss. The composite with 50 vol% modified PMN–PT held 3 times energy density more than P(VDF-HFP) at 80 kV/mm. The results obtained in this study would be

helpful in exploring potential dielectric materials in the application for energy storage.

The manuscript was written through contributions of all authors. All authors have given approval to the final version of the manuscript

Acknowledgements

This work was financially supported by Graduate Student Research Innovation Project in Hunan Province (no. 150140011), Ph.D. Programs Foundation of Ministry of Education of China (no. 20110162110044), and State Key Laboratory of Powder Metallurgy, Central South University, Changsha, China.

Reference

- 1 S. Liu, S. Xue, W. Zhang, J. Zhai and G. Chen, *J. Mater. Chem. A*, 2014, **2**, 18040-18046.
- 2 H. Tang and H. A. Sodano, *Nano Lett.*, 2013, **13**, 1373-1379.
- 3 B. Chu, X. Zhou, K. Ren, B. Neese, M. Lin, Q. Wang, F. Bauer and Q. M. Zhang, *Science*, 2006, **313**, 334-336.
- 4 Z. D. Liu, Y. Feng and W. L. Li, *RSC Adv.*, 2015, **5**, 29017-29021.
- 5 V. K. Thakur, G. Ding, J. Ma, P. S. Lee and X. Lu, *Adv. Mater.*, 2012, **24**, 4071-4096.
- 6 H. Luo, D. Zhang, C. Jiang, X. Yuan, C. Chen and K. Zhou, *ACS Appl. Mater. Interfaces*, 2015, **7**, 8061-8069.
- 7 S. Wu, W. Li, M. Lin, Q. Burlingame, Q. Chen, A. Payzant, K. Xiao and Q. M. Zhang, *Adv. Mater.*, 2013, **25**, 1734-1738.

- 8 V. K. Thakur, E. J. Tan, M.-F. Lin and P. S. Lee, *J. Mater. Chem.*, 2011, **21**, 3751-3759.
- 9 D. Yuan, Z. Li, W. Thitsartarn, X. Fan, J. Sun, H. Lia and C. He, *J. Mater. Chem. C*, 2015, **3**, 3708-3713.
- 10 M.-F. Lin, V. K. Thakur, E. J. Tan and P. S. Lee, *J. Mater. Chem.*, 2011, **21**, 16500-16504.
- 11 V. K. Thakur, M.-F. Lin, E. J. Tan and P. S. Lee, *J. Mater. Chem.*, 2012, **22**, 5951-5959.
- 12 V. K. Thakur, J. Yan, M.-F. Lin, C. Zhi, D. Golberg, Y. Bando, R. Sim and P. S. Lee, *Poly. Chem.*, 2012, **3**, 962-969.
- 13 V. K. Thakur, E. J. Tan, M.-F. Lin and P. S. Lee, *Poly. Chem.*, 2011, **2**, 2000-2009.
- 14 K. Yang, X. Huang, Y. Huang, L. Xie and P. Jiang, *Chem. Mater.*, 2013, **25**, 2327-2338.
- 15 H. Tang, Y. Lin and H. A. Sodano, *Adv. Energy Mater.*, 2012, **2**, 469-476.
- 16 C. Ehrhardt, C. Fettkenhauer, J. Glenneberg, W. Münchgesang, H. S. Leipner, G. Wagner, M. Diestelhorst, C. Pientschke, H. Beige and S. G. Ebbinghaus, *RSC Adv.*, 2014, **4**, 40321-40329.
- 17 H. Luo, D. Zhang, L. Wang, C. Chen, J. Zhou and K. Zhou, *RSC Adv.*, 2015, **5**, 52809-52816.
- 18 Y. Zhang, G. Gao, H. L. W. Chan, J. Dai, Y. Wang and J. Hao, *Adv. Mater.*, 2012, **24**, 1729-1735.

- 19 X. Fu, I. I. Naumov and H. Fu, *Nano Lett.*, 2013, **13**, 491-496.
- 20 O. Auciello, J. F. Scott, R. Ramesh, *Phys. Today* 1998, **51**, 22-27.
- 21 H. X. Tang and H. A. Sodano, *Appl. Phys. Lett.*, 2013, **102**, 063901.
- 22 S. Tong, B. Ma, M. Narayanan, S. Liu, R. Koritala, U. Balachandran and D. Shi, *ACS Appl. Mater. Interfaces*, 2013, **5**, 1474-1480.
- 23 R. E. Cohen, *Nature*, 2006, **441**, 941-942.
- 24 E. Brown, C. Ma, J. Acharya, B. Ma, J. Wu and J. Li, *ACS Appl. Mater. Interfaces*, 2014, **6**, 22417-22422.
- 25 X. Hao, Y. Wang, J. Yang, S. An and J. Xu, *J. Appl. Phys.*, 2012, **112**, 114111-114111-6.
- 26 L. Wu, X. Wang, H. Gong, Y. Hao, Z. Shen and L. Li, *J. Mater. Chem. C*, 2015, **3**, 750-758.
- 27 Y. Song, Y. Shen, H. Liu, Y. Lin, M. Li and C.-W. Nan, *J. Mater. Chem.*, 2012, **22**, 8063-8068.
- 28 M.-F. Lin, V. K. Thakur, E. J. Tan and P. S. Lee, *RSC Adv.*, 2011, **1**, 576-578.
- 29 H. Lee, S. M. Dellatore, W. M. Miller and P. B. Messersmith, *Science*, 2007, **318**, 426-430.
- 30 Q. Yue, M. Wang, Z. Sun, C. Wang, C. Wang, Y. Deng and D. Zhao, *Journal of Materials Chemistry B*, 2013, **1**, 6085-6093.
- 31 C. Chao, J. Liu, J. Wang, Y. Zhang, B. Zhang, Y. Zhang, X. Xiang and R. Chen, *ACS Appl. Mater. Interfaces*, 2013, **5**, 10559-10564.
- 32 B. Luo, X. Wang, Y. Wang and L. Li, *J. Mater. Chem. A*, 2014, **2**, 510-519.

- 33 P. Hu, Y. Song, H. Liu, Y. Shen, Y. Lin and C.-W. Nan, *J. Mater. Chem. A*, 2013, **1**, 1688-1693.
- 34 S. P. Fillery, H. Koerner, L. Drummy, E. Dunkerley, M. F. Durstock, D. F. Schmidt and R. A. Vaia, *ACS Appl. Mater. Interfaces*, 2012, **4**, 1388-1396.
- 35 Z. M. Dang, H. Y. Wang, Y. H. Zhang and J. Q. Qi, *Macromol. Rapid Commun.*, 2005, **26**, 1185-1189.
- 36 L. L. Sun, B. Li, Y. Zhao, G. Mitchell and W. H. Zhong, *Nanotechnology*, 2010, **21**, 305702.
- 37 X. He, K. Yao and B. K. Gan, *J. Appl. Phys.*, 2005, **97**, 084101.
- 38 L. Xie, X. Huang, K. Yang, S. Li and P. Jiang, *J. Mater. Chem. A*, 2014, **2**, 5244-5251.
- 39 K. Yu, Y. Niu, Y. Zhou, Y. Bai and H. Wang, *J. Am. Ceram. Soc.*, 2013, **96**, 2519-2524.
- 40 B. Chu, M. Lin, B. Neese and Q. Zhang, *J. Appl. Phys.*, 2009, **105**, 014103.
- 41 X. Hao, J. Zhai and X. Yao, *J. Am. Ceram. Soc.*, 2009, **92**, 1133-1135.
- 42 K. Yang, X. Huang, L. Xie, C. Wu, P. Jiang and T. Tanaka, *Macromol. Rapid Commun.*, 2012, **33**, 1921-1926.

TOC:

Dielectric properties and energy storage density in poly(vinylidene

fluoride-co-hexafluoropropylene) were enhanced by surface-functionalized relaxor ferroelectric ceramic $\text{Pb}(\text{Mg}_{1/3}\text{Nb}_{2/3})\text{O}_3\text{-PbTiO}_3$.

